Desalination 444 (2018) 142–150

Contents lists available at ScienceDirect

Desalination

journal homepage: www.elsevier.com/locate/desal

Investigation of the hydrogen evolution phenomenon on $CaCO_3$ precipitation in artificial seawater

Milad Piri, Reza Arefinia*

Chemical Engineering Department, Faculty of Engineering, Ferdowsi University of Mashhad, Mashhad, Iran

ARTICLE INFO

Keywords:
Deposition
Hydrogen evolution
Calcium carbonate
Cathodic potential

ABSTRACT

Precipitation of $CaCO_3$, as the most important part of scales, causes a serious problem in industrial equipment such as pipelines and desalination plants. The effect of the hydrogen evolution phenomenon on the electrochemical precipitation was studied through varying different factors including cathodic potential (CP), bicarbonate concentration, and solution temperature. The application of CP from $-0.8\ V_{SCE}$ to $-1.2\ V_{SCE}$, an increase in bicarbonate concentration and temperature elevation from 25 °C to 45 °C led to the increase of scaling time (t_s) and residual current density (i_r). In all cases, it was indisputably found that the hydrogen evolution phenomenon had a predominant effect on the calcium carbonate precipitation. The surface analyses by means of scanning electron microscopy (SEM) showed formation of crystals in two defined forms of calcite and aragonite. Moreover, the energy dispersive spectroscopy (EDS) technique confirmed the formation of $CaCO_3$ crystals.

1. Introduction

Many activities have been performed to reduce the precipitation phenomenon [1,2]. Formation of mineral scales on the internal wall of heat exchangers, boilers, cooling water systems, and desalination plants reduces the tube's diameter, causes significant decrease in heat transfer efficiency and may be occasionally lead to the shutdown of the industrial plant [3,4].

Cathodic protection is an effective method to reduce the corrosion process in desalination unites. However, one major problem associated with cathodic protection is that it can lead to the formation of mineral scales known as “calcareous deposits” whose major constituent is calcium carbonate ($CaCO_3$) [5,6]. Mineral scales, mainly as $CaCO_3$, may cause serious problems such as pitting corrosion or failure in the structural metal of equipment [7].

To evaluate the precipitation process, the experiments must be run in conditions similar to the actual operating system conditions. However, this takes a lot of time [8]. Therefore, certain procedures of scaling study have been based on the acceleration of calcareous precipitation. Among them, some are chemical using materials such as sodium hydroxide and sodium carbonate [9], whereas some others are electrochemical techniques such as chronoelectrogravimetry, impedancemetry and chronoamperometry [6,10–13]. Electrochemical precipitation occurs in a very thin layer on the electrode surface, contrary to chemical precipitation that occurs in the whole solution [14]. Indeed, electrochemical methods are based on the increase of the interfacial pH of the metal caused by oxygen and water reduction reactions as a result of the application of cathodic potential (CP). Then, the concentration of carbonate ions increases according to the following reaction [15]:

$$HCO_3^- + OH^- \rightarrow CO_3^{2-} + H_2O \quad (1)$$

Afterward, the increase of carbonate concentration induces the $CaCO_3$ scaling as [7,15]:

$$CO_3^{2-} + Ca^{2+} \rightarrow CaCO_{3\,(s)} \quad (2)$$

The influence of different parameters such as seawater composition [2,5,6,11,16,17], flow rate of solution [18–23], pH of solution (pH_s) [21] and solution temperature [6,11,17,21,22] have been studied on the formation and characteristics of calcareous scales. However, mainly due to the various compositions of seawater solution used and substrates considered, some contradictory results and conclusions have been reported [11]. It is well known that calcium carbonate is the major constituent of scales and understanding its deposition mechanism is very important. Barchiche et al. proposed that in the absence of Mg^{2+}, calcium carbonate deposits in two crystalline forms: calcite and aragonite on gold [2]. Benslimane et al. studied the inhibition effect of Zn^{2+} on $CaCO_3$ precipitation in a synthetic CalcoCarbonically pure (CCP) solution [12]. Some other researchers have investigated the calcareous scaling in artificial seawater based on standard ASTM D1141 [5,11]. In these works, the mechanism of $CaCO_3$ precipitation is affected by the contribution of other types of scales such as $Mg(OH)_2$ [2]

* Corresponding author at: Chemical Engineering Department, Faculty of Engineering, Ferdowsi University of Mashhad, Mashhad, Iran.
E-mail address: arefinia@um.ac.ir (R. Arefinia).

https://doi.org/10.1016/j.desal.2018.05.018
Received 30 January 2018; Received in revised form 8 May 2018; Accepted 22 May 2018
Available online 28 May 2018

as well as the presence of other ions such as SO_4^{2-} and Ca^{2+} [11]. Deslouis et al. characterized calcareous deposits on gold electrode in artificial seawater in the absence of $Mg(OH)_2$ and in hydrodynamic conditions [18].

Deposition process under the application of CP is commonly associated with the hydrogen evolution phenomenon due to water reduction reaction. Okstad et al. reported the significant effect of hydrogen bubbling on calcareous deposits during cathodic protection [19]. Nevertheless, the effect of hydrogen evolution on the precipitation of $CaCO_3$ in the absence of interfering ions like Mg^{2+} and SO_4^{2-} on the surface of carbon steel calls for further investigation.

The main objective of the present research was to study the hydrogen evolution phenomenon associated with $CaCO_3$ scale formation under the application of CP and in the absence of the formation of other scales like $Mg(OH)_2$. Moreover, the effect of CP, bicarbonate concentration, and solution temperature on the $CaCO_3$ precipitation was investigated. In so doing, artificial seawater was prepared based on seawater according to ASTM D1141. The characteristics of the $CaCO_3$ scale deposited in different conditions were thoroughly evaluated by means of electrochemical methods including chronoamperometry, current-voltage and electrochemical impedance spectroscopy (EIS). To clarify the significance of the hydrogen evolution phenomenon, the deposition conditions were also evaluated from a chemical view point based on the thermodynamic equilibrium of ion concentrations. Finally, the morphology and type of $CaCO_3$ crystals formed on carbon steel were studied using scanning electron microscopy (SEM) and their constituent elements were identified using the energy dispersive spectroscopy (EDS) technique.

2. Experimental

2.1. Solution and electrode preparation

To evaluate the precipitation mechanism of calcium carbonate in the absence of other forms of scales, the basic artificial seawater was prepared by incorporation of $NaHCO_3$ 0.20 g/L and $CaCl_2$ 1.16 g/L corresponding to ASTM D1141. The initial pH_s value was adjusted to 8.2 by NaOH. All chemicals were reagent grades purchased from Merck (Germany).

The effect of bicarbonate concentration on precipitation was studied by incorporation of 50, 100 and 200% bicarbonate according to ASTM D1141, which is equal to 0.1, 0.2 and 0.4 g/L within the artificial solution, respectively. The effect of temperature (25, 35 and 45 °C) on precipitation was investigated at -1.0 V_{SCE} in the basic artificial solution. The solution temperature was kept constant using a water bath with an accuracy of ± 1 °C.

The chemical composition of carbon steel as the working electrode with an area of 1 cm^2 is given in Table 1The specimens were mechanically abraded with emery papers of 800, 1200 and 2000, respectively. The specimens were, then, thoroughly washed with double distilled water and acetone.

2.2. Electrochemical techniques

2.2.1. Electrochemical cell

All electrochemical measurements were performed by using a potentiostat/galvanostat (Autolab) 302 N instrument in a three-electrode cell including a graphite rode with a large surface area as the counter electrode, a saturated calomel electrode (SCE) as the reference electrode and carbon steel as the working electrode. Solution tests were open to the atmosphere under unstirred conditions.

Table 1
The chemical composition of carbon steel.

Element	C	Mn	P	S	Si	Cr	Cu	Mo	Ni	V
Composition (wt%)	0.35	1.06	0.04	0.04	0.10	0.40	0.40	0.15	0.40	0.08

2.2.2. Chronoamperometry and cathodic polarization

The kinetics of calcium carbonate deposition was monitored using the chronoamperometry technique at different CPs (-0.8, -0.9, -1.0, -1.1 and -1.2 V_{SCE}) with a signal record interval of 2 s. For better understanding the cathodic reactions that occur at the surface of carbon steel, current-potential curves were recorded with a scan rate of 1 mV s^{-1} in the potential range from -0.6 to -1.80 V_{SCE} in the artificial seawaters with different bicarbonate concentrations and different solution temperatures at pH = 8.2.

2.2.3. Electrochemical impedance spectroscopy

The nature of $CaCO_3$ scale deposited on the electrode surface was studied using the electrochemical impedance spectroscopy (EIS) test. To this end, the applied CP was kept on the electrode and the EIS spectra were recorded around this potential at an amplitude perturbation of 10 mV over the frequency range of 100 kHz to 10 mHz after performing the chronoamperometry test.

2.3. Characterization of deposited film

Ex-situ characterization of $CaCO_3$ precipitation was performed using the scanning electron microscope (SEM, LEO 1450VP) technique after the formation of a scale film under CP runs and the elements nature present in the scale layer was determined using the energy dispersive spectroscopy (EDS) technique.

3. Results and discussion

3.1. Evaluation of tendency to chemical precipitation of $CaCO_3$

It may be useful to evaluate the tendency of $CaCO_3$ precipitation on carbon steel surface in the artificial seawater before applying CP (possibility of chemical deposition). The dissolution equilibrium of $CaCO_3$ is as follows [24]:

$$CaCO_{3(s)} \leftrightarrow CO_3^{2-}{}_{(aq)} + Ca^{2+}{}_{(aq)} \quad (3)$$

According to this equation, it can be found that $CaCO_3$ precipitation takes place when the concentration of both Ca^{2+} and CO_3^{2-} becomes greater than the solubility (S) of calcium carbonate at a determined pH_s and temperature. In this regard, the value of S is calculated by the help of following equation [24,25]:

$$S = \left(\frac{K_{sp}(10^{-2pH_s} + K_1 . 10^{-2pH_s} + K_1K_2}{K_1K_2} \right)^{0.5} \quad (4)$$

where K_1 and K_2 are the acid dissociation constants for H_2CO_3 and HCO_3^-, respectively and K_{sp} is the solubility product constant of $CaCO_3$. The constants K_1, K_2 and K_{sp} are functions of temperature, which have been calculated using the following relations [26,27]:

$$pK_1 = 10^{-4}\, T^2 - 1.22\, T + 6.5755 \quad (5)$$

$$pK_2 = 9.0 \times 10^{-5}\, T^2 - 0.0137\, T + 10.618 \quad (6)$$

$$pK_{sp} = 0.031111\, T + 1502.0\, T^{-1} - 5.518\, \log T + 7.8156 \quad (7)$$

The values of K_1, K_2 and K_{sp} at 25 °C were calculated using Eqs. (5)–(7) and they were 4.94×10^{-7}, 4.06×10^{-11} and 4.63×10^{-9}, respectively. Before applying CP, the pH value was equal to 8.2 throughout the solution even at the electrode/solution interface. Thus, the solubility of $CaCO_3$ was calculated as 85.6 ppm at 25 °C by Eq. (4).

Besides, it is essential to determine the concentration of both carbonate (CO_3^{2-}) and calcium (Ca^{2+}) ions within the solution. The concentration of Ca^{2+} is high enough (1160 ppm) while the

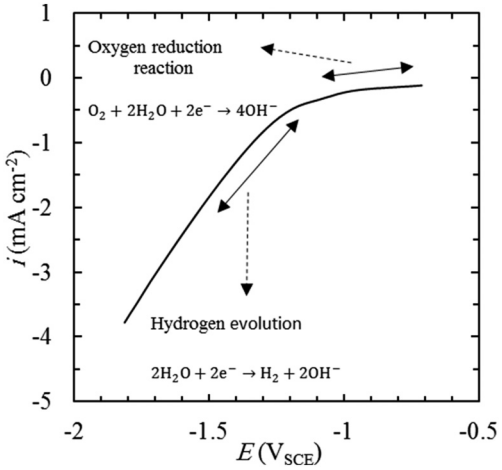

Fig. 1. Current-potential curve of carbon steel in artificial seawater based on ASTM D1141 ($NaHCO_3$ 201 ppm and $CaCl_2$ 1160 ppm) at 25 °C. Scan rate: 1 mV s^{-1}.

concentration of CO_3^{2-} has a limiting effect on $CaCO_3$ precipitation. In this work, CO_3^{2-} ions were generated through the dissolution of $NaHCO_3$ and their concentration was calculated by using the following equation [25]:

$$[CO_3^{2-}] = \frac{K_1 K_2 [HCO_3^-]}{10^{-2pH_s} + 10^{-pH_s} K_1 + K_1 K_2} \quad (8)$$

Regarding this equation, the concentration of carbonate ions is equal to 1.3 ppm within the solution at a pH_s = 8.2 and at a temperature of 25 °C. As a result, the greater value of calcium carbonate solubility (S = 85.6 ppm) compared with CO_3^{2-} concentration (1.3 ppm) indicates that chemical deposition of $CaCO_3$ within the artificial seawater is not possible to take place.

3.2. Evaluation of electrochemical precipitation of $CaCO_3$

3.2.1. Current-potential curve

Fig. 1 shows the current-potential curve for carbon steel at pH_s = 8.2 and at a temperature of 25 °C. Two distinct regions can be identified as the slope of the curve considerably increases at a potential range between −1.0 and −1.1 V_{SCE}. The first region at more positive potentials involves the oxygen reduction reaction as shown by the following Eq. [15]:

$$O_2 + 2H_2O + 2e^- \rightarrow 4OH^- \quad (9)$$

In the second region created at more negative potentials, the water reduction reaction along with hydrogen evolution occurs as [15]:

$$2H_2O + 2e^- \rightarrow H_2 + 2OH^- \quad (10)$$

Under the application of CPs, the production of hydroxyl groups corresponding to Eqs. (9) and (10) involves an increase in the pH value in the vicinity of the electrode, causing the dissociation of bicarbonate anions and their transformation into carbonate anions according to Eq. (1). The increase of CO_3^{2-} concentration forces the carbonate calcium precipitation on the carbon steel surface according to Eq. (2). Moreover, the value of pH_s was measured after the electrochemical test and the obtained results suggest no change in the solution pH most probably due to both the buffer nature of artificial seawater and the small volume of the solution around the electrode surface compared to that of bulk solution.

It is clear from Fig. 1 that the cathodic current in the region corresponding to water reduction is considerably higher than that of oxygen reduction. This can be explained by high dependency of oxygen reduction on the diffusion phenomenon of oxygen molecules within the solution, which may restrict the rate of this reaction.

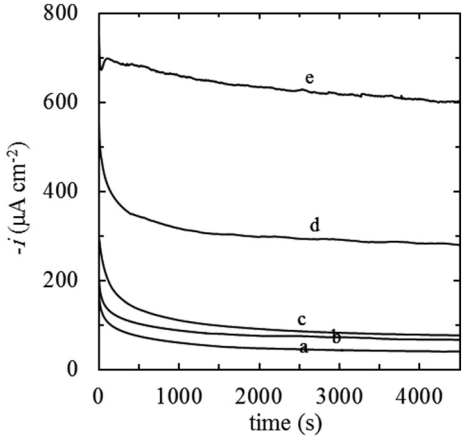

Fig. 2. Chronoamperometric curves of carbon steel in artificial seawater based on ASTM D1141 at 25 °C and at different cathodic potentials: (a) – 0.8 V_{SCE}, (b) – 0.9 V_{SCE}, (c) – 1.0 V_{SCE}, (d) – 1.1 V_{SCE} and (e) −1.2 V_{SCE}.

3.2.2. Chronoamperometry

Electrochemical scaling is induced by the application of different CPs on the electrode surface [9]. Fig. 2 shows the chronoamperometric curves for carbon steel at different CPs in artificial seawater based on ASTM D1141 at 25 °C. As can be seen, in all CPs, the current density decreases immediately under progressive blockage of the metal surface by $CaCO_3$ precipitation. After a certain time, known as scaling time (t_s), variation of current density with time becomes negligible, indicating the end of the growth stage of $CaCO_3$ crystals [10,28]. In this work, the scaling time was determined by drawing the tangent to the inflexion point of the chronoamperometric curve and the point where it crosses the time axis was considered as an approximated scaling time, t_s. Under longer time of CP application, a steady state current, named residual current density (i_r), is attained as a result of an almost total coverage of the electrode surface. The estimated values of the scaling parameters (t_s and i_r) for carbon steel at different CPs are given in Table 2.

Table 2 shows that both residual current density, i_r, and scaling time, t_s, increase continuously as the CP shifts to more negative values. A similar behavior has been reported elsewhere [19,22]. The parameter i_r is an important feature of the $CaCO_3$ scale deposited on the metal surface and its higher value is an evidence of the formation of a weaker layer of deposits.

The value of i_r consists of two currents: oxygen and water reduction. When the CP value shifts towards the negative values, the contribution of oxygen reduction to the i_r decreases and that of water reduction increases [19], as shown in the current-voltage curve (Fig. 1). In addition, the higher rate of water reduction reaction compared with that of oxygen reduction induces a more significant effect of water reduction on the precipitation parameters under electrochemical deposition, especially at CPs > −1.0 V_{SCE}. In view of the water reduction reaction Eq. (10), it can be concluded that the application of more negative CPs produces a higher rate of both hydroxyl groups and hydrogen bubbling.

It is known that an increase in the concentration of hydroxyl groups near the electrode surface favors $CaCO_3$ deposition process. To inspect the effect of interfacial pH on the scaling process under the application of CP, it is essential to determine the values of pH adjacent to the electrode surface; however, it is usually difficult to measure. In this

Table 2
Effect of cathodic potential on the scaling parameter of carbon steel in artificial seawater based on ASTM D1141 at 25 °C.

CP (V_{SCE})	−0.8	−0.9	−1.0	−1.1	−1.2
t_s (s)	470	690	1140	1840	4140
i_r (μA cm^{-2})	41	68	77	281	602

Table 3
Effect of CP on the interfacial pH, $CaCO_3$ solubility and carbonate concentration in artificial seawater based on ASTM D1141 at a solution pH of 8.2 and at a temperature of 25 °C.

CP (V_{SCE})	−0.8	−0.9	−1.0	−1.1	−1.2
Interfacial pH (Tlili et al. [14])	9.70	9.80	9.85	9.87	9.90
S (ppm) according to Eq. (4)	16.6	15.1	14.4	14.2	13.8
$[CO_3^{2-}]$ (ppm) according to Eq. (8)	34.0	41.0	44.9	46.5	49.0

regard, some works have been carried out to measure the interfacial pH in various conditions [14,29]. Tlili et al. [14] studied $CaCO_3$ precipitation process by measuring the interfacial pH by varying CP in a solution similar to that used in the present work under hydrodynamic conditions. However, they found that hydrodynamic conditions have a negligible influence on the measured values of interfacial pH. According to them, here, the variation of interfacial pH under the application of different CPs at a solution pH of 8.2 and temperature of 25 °C is presented in.

Table 3. Then, the values of $CaCO_3$ solubility (S) and carbonate concentration ($[CO_3^{2-}]$) were calculated according to Eq. (4) and Eq. (8), respectively. However, it is also important to note that as the electrochemical precipitation takes place close to the electrode surface, the interfacial pH values were substituted for parameter pH_s in these equations.

The lower value of S than $[CO_3^{2-}]$ at all CPs verifies the precipitation of $CaCO_3$. However, it is evident that the values of S decrease while the values of $[CO_3^{2-}]$ increase adjacent to the electrode surface as the interfacial pH increases. This suggests that the application of more negative CP favors $CaCO_3$ precipitation on the electrode surface and thus one may expect reduction in the value of i_r and t_s, however, inspection of results presented in Table 2 shows an opposite trend of variation. This contradiction can be mainly attributed to the interference of the hydrogen bubbling phenomenon, which is associated with the water reduction reaction. In the other words, the increment of t_s and i_r with the application of more negative CP indicates that the effect of the hydrogen evolution phenomenon on the scale deposition overcomes that of the increase in the interfacial pH.

The predominant effect of the hydrogen evolution phenomenon can be explained in terms of scaling parameters. The increase in i_r with the application of a more negative value of CP can be attributed to the induction of higher porosity in the structure of the scale layer and detachment of the small fragment, as discussed earlier [2].This causes the lower coverage of scale deposition on the metal surface and, consequently, the higher value of residual current density [11,22]. Also, an increase in scaling time, t_s can be ascribed to a decrease in the rate of crystal growth on the carbon steel surface. Indeed, the hydrogen bubbling phenomenon decreases the likelihood of precipitation reaction occurring on the nucleated sites of $CaCO_3$ crystals even under the condition of $CaCO_3$ oversaturation, thus, enhancing the required time to reach full growth of scale crystals.

3.2.3. EIS measurement

The main effect of hydrogen evolution on the characteristics of the $CaCO_3$ scale formed under potentiostatic runs were immediately studied using the EIS technique at the applied CP. The recorded data in the form of Nyquist and phase Bode plots are presented in Fig. 3. As can be seen, Nyquist plots consist of two impressed semi-circles; the one at high frequencies has a larger diameter and corresponds to the characteristics of the deposit layer while the one at low frequencies corresponds to the reduction of reaction feature at the metal/deposit layer interface [13]. The impedance plots were well fitted to the electrical circuit containing two time constants as shown in Fig. 4.

In this circuit, R_s, R_f and R_{ct} represent solution resistance, deposit film resistance and charge transfer resistance, respectively. The elements of CPE_f and CPE_{dl} correspond to the constant phase elements of the deposit film and the double layer, respectively [4]. The constant phase element (CPE) is substituted for the ideal capacitance element to better fit the EIS curves when the Nyquist circle is in the form of a depressed shape. This is mainly affected by the surface heterogeneity such as surface roughness, surface impurity, accumulation of corrosion products and formation of a porous layer. The impedance of the CPE is represented by the following expression [10]:

$$Z_{CPE} = (Y(j\omega)^n)^{-1} \quad (11)$$

where Y is admittance coefficient with a dimension of $\Omega^{-1}\,s^n\,cm^{-2}$, ω is the angular frequency (rad/s), n is a power constant as a measure of surface inhomogeneity and j defines the imaginary number ($\sqrt{-1}$). Using this relation, the impedance of both CPE_f and CPE_{dl} can be defined where Y_f and Y_{dl} correspond to admittance coefficient of the deposit film and the double layer, respectively; n_f and n_{dl} are power constants for the scale film and the double layer, respectively.

All the EIS spectra were well-fitted to the equivalent circuit using the Zview software and the calculated parameters are summarized in Table 4. It can be found that when the CP shifts towards negative values, the film resistance (R_f) decreases markedly, and the parameter n_f decreases. These trends of variation indicate the lower strength and higher porosity level of the $CaCO_3$ scale film as a result of a higher rate of hydrogen evolution, which is in full agreement of the results obtained by chronoamperometry tests. Moreover, the admittance coefficient (Y_f) increases, again confirming that hydrogen bubbling hinders the total coverage of metal surface and the porous structure of the scale film facilitates the penetration of solution molecules within the scale film structure.

The data in Table 4 show while the charge transfer resistance (R_{ct}) decreases, the double layer admittance (Y_{dl}) increases as a result of the application of more negative CP, indicating the facilitation of cathodic reaction. This behavior can be attributed to the effect of the hydrogen evolution on the structure of the scale film. Indeed, $CaCO_3$ deposits have a physical barrier effect against the penetration of both oxygen and water molecules; thus, incomplete coverage of metal surface promotes diffusion of these components towards the metal surface. Therefore, the higher concentration of oxygen and water molecules at the interface of metal/$CaCO_3$ deposit causes an increase in the reaction rate of cathodic reductions. The decrease in the parameter n_{dl} is ascribed to the increase in the nonhomogeneity of the metal surface.

Consequently, the EIS data on the nature of the $CaCO_3$ scale precipitated at different CPs well explains the results obtained by chronoamperometry tests and it can be stated that the increase of residual current density, i_r, is attributed to the lower coverage or higher porosity level of $CaCO_3$ scale film. This evidence verifies the inhibiting effect of the hydrogen evolution phenomenon on the formation of $CaCO_3$ deposits.

3.3. Effect of bicarbonate concentration at CP = −1.0 V_{SCE}

Fig. 5 shows the chronoamperometric curves for carbon steel in the artificial solution with different concentrations of bicarbonate including 50%, 100% and 200% corresponding to ASTM D1141 ($[HCO_3^-]_{Std}$) at CP = −1.0 V_{SCE} and 25 °C. The values of t_s and i_r are found respectively to be about 920 s and 62 μA cm^{-2} for 50%, 2230 s and 153 μA cm^{-2} for 200% $[HCO_3^-]_{Std}$. The values of these parameters for 100% $[HCO_3^-]_{Std}$ have been reported in Table 2. It is clear that the increase of $[HCO_3^-]$ results in an increase in the values of both parameters i_r and t_s.

Before going on any further to consider the electrochemical evidence in more detail, it can be useful to analyze the effect of chemical composition of the solution on $CaCO_3$ deposition. It was reported earlier that a change in the bicarbonate concentration, especially at high concentrations, has a negligible effect on the pH of the solution because of the fact that the artificial solution acts as a buffer [25]. In the present

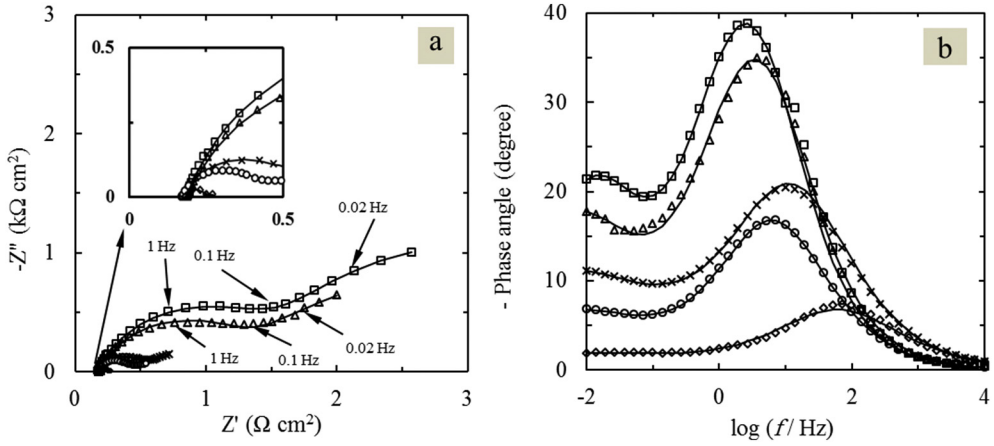

Fig. 3. (a) Nyquist and (b) Bode phase plots for deposit covered carbon steel specimens in artificial seawater based on ASTM D1141 at 25 °C and at different CPs: (□) – 0.8 V_{SCE}, (Δ) – 0.9 V_{SCE}, (×) – 1.0 V_{SCE}, (○) – 1.1 V_{SCE}, (◊) –1.2 V_{SCE}, (—) fitting line.

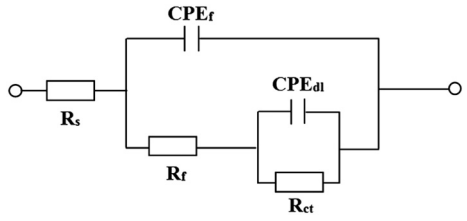

Fig. 4. Equivalent circuit model used to analyze impedance data.

Table 4
Effect of cathodic potential on the scaling parameter of carbon steel in artificial seawater based on ASTM D1141 at 25 °C.

CP (V_{SCE})	R_f ($\Omega\,cm^2$)	CPE_f		R_{ct} ($\Omega\,cm^2$)	CPE_{dl}	
		$Y_f \times 10^4$ ($\Omega^{-1}\,cm^{-2}\,s^n$)	n_f		$Y_{dl} \times 10^4$ ($\Omega^{-1}\,cm^{-2}\,s^n$)	n_{dl}
−0.8	1460	2.16	0.78	2960	38.1	0.71
−0.9	1210	2.28	0.79	2810	47.7	0.62
−1.0	360	4.16	0.74	730	110.0	0.54
−1.1	280	4.37	0.70	310	130.0	0.52
−1.2	80	5.81	0.67	40	654.0	0.51

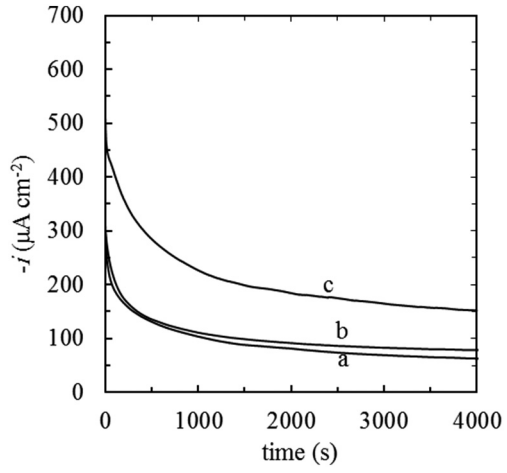

Fig. 5. Chronoamperometric curves of carbon steel in artificial seawater based on ASTM D1141 at 25 °C with different bicarbonate concentrations: (a) 50% $[HCO_3^-]_{Std}$, (b) 100% $[HCO_3^-]_{Std}$ and (c) 200% $[HCO_3^-]_{Std}$.

work, the values of pH_s at different concentrations of bicarbonate were measured and found to be very close to the value of 8.2. In this situation, an increase in $[CO_3^{2-}]$ with $[HCO_3^-]$ is expected according to Eq. (1), however, the constant pH of the solutions implies that the $[HCO_3^-]/[CO_3^{2-}]$ ratio still remains constant.

Considering Eq. (2), it may be expected that the increase of $[CO_3^{2-}]$ favors $CaCO_3$ deposition on the carbon steel surface, hence, decreasing the current density. However, the opposite has occurred and residual current density, i_r increases according to the chronoamperometric runs. This can be explained by the fact that direct reduction of bicarbonate ions takes place concurrently with oxygen and water, especially at high $[HCO_3^-]$, according to the following equation [30,31]:

$$2HCO_3^- + 2e^- \rightarrow H_2 + 2CO_3^- \quad (12)$$

The effect of $[HCO_3^-]$ on the cathodic current density is analyzed by current-potential curves in Fig. 6. It is obvious that cathodic current density is increased by incorporation of a higher content of bicarbonate within the solution. Moreover, the increase in cathodic current density is more significant at more negative potentials. Considering Eq. (12), the increase of $[HCO_3^-]$ provides the higher rate of hydrogen evolution on the metal surface [31]. This suggests that the hydrogen bubbles interfere in the stages of the formation of the $CaCO_3$ deposit on the surface of carbon steel. The increase of t_s with bicarbonate concentration indicates the longer time of growing stage and the increase in i_r implies the incomplete coverage of the carbon steel surface or a decrease in the compaction of the $CaCO_3$ scale layer as a result of the hydrogen bubbling phenomenon. The low degree of surface coverage may also be related to the effect of the hydrogen bubbling on the nucleation stage of scale formation by sequestering calcium carbonate to

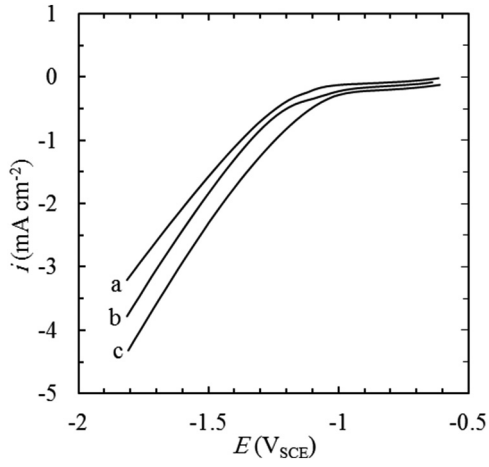

Fig. 6. Current-potential curves for carbon steel specimens in artificial seawater based on ASTM D1141at 25 °C with different bicarbonate concentrations: (a) 50% $[HCO_3^-]_{Std}$, (b) 100% $[HCO_3^-]_{Std}$ and (c) 200% $[HCO_3^-]_{Std}$. Scan rate:1 mV s^{-1}.

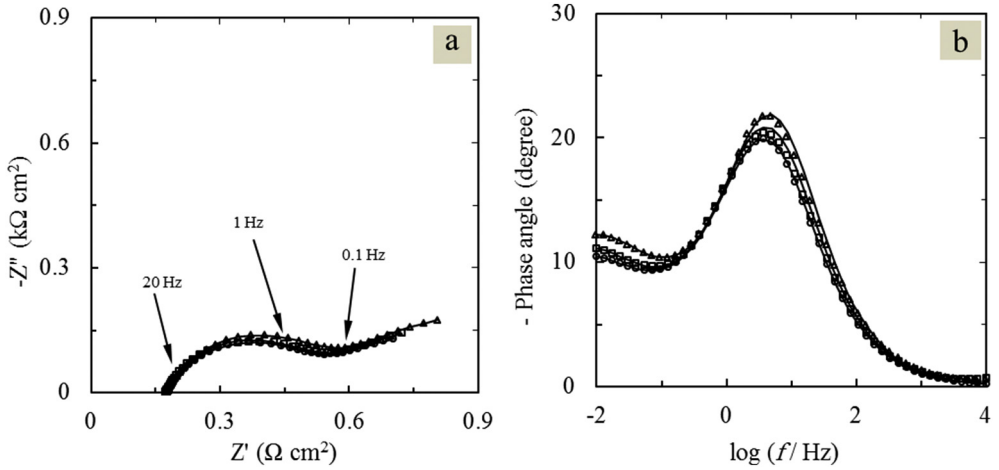

Fig. 7. (a) Nyquist and (b) Bode phase plots for deposit covered carbon steel samples at 25 °C with different bicarbonate concentrations: (Δ) 50% $[HCO_3^-]_{Std}$, (□) 100% $[HCO_3^-]_{Std}$, (○) 200% $[HCO_3^-]_{Std}$ and (—) fitting line.

precipitate on the metal surface.

The nature of the $CaCO_3$ film deposited at CP = −1.0 V_{SCE} in artificial seawater with different bicarbonate concentrations was studied by using the EIS method and the impedance curves are shown in Fig. 7. The EIS data were well-fitted to the electrical circuit, as shown in Fig. 4 and the obtained impedance parameters are presented in Table 5.

It can be found that an increase in bicarbonate concentration causes a decrease in the solution resistance within the pores of the deposit layer in terms of R_f and a decrease in resistance against reduction reaction in terms of R_{ct}. Moreover, the values of both Y_f and Y_{dl} increase mainly due to the increase in the water content both within the scale layer and at the metal/deposit interface, respectively. In addition, reduction of both parameters n_f and n_{dl} suggests a higher degree of porosity of the $CaCO_3$ scale film and the increment of the nonhomogeneity of the metal/deposit interface, respectively. These observations indicate decrease in the strength of the scale deposit and its higher level of porosity on the metal surface due to the hydrogen evolution phenomenon, which makes perfect sense in view of the increase of i_r with bicarbonate concentration obtained from chronoamperometric runs.

Considering these results, it can be stated that an increase in bicarbonate concentration under the application of CP ≤ −1.0 V_{SCE} favors the reduction of $CaCO_3$ precipitation at a determined pH and temperature. However, it is more significant at a higher concentration of bicarbonate as the i_r for 200% $[HCO_3^-]_{Std}$ is approximately 2.5 times greater than that of 50% at CP = −1.0 V_{SCE} and temperature 25 °C.

3.4. Effect of solution temperature at CP = −1.0 V_{SCE}

In industrial applications, temperature is an important factor that might vary within a relatively wide range during the operational time. Moreover, the solution temperature may have a significant effect on the scaling process of the equipment. Fig. 8 shows the chronoamperometric curves of carbon steel cathodically polarized at CP = −1.0 V_{SCE} in artificial seawater at different solution temperatures. At temperatures of 25, 35 and 45 °C, the values of t_s are equal to 1140, 1580 and 2120 s,

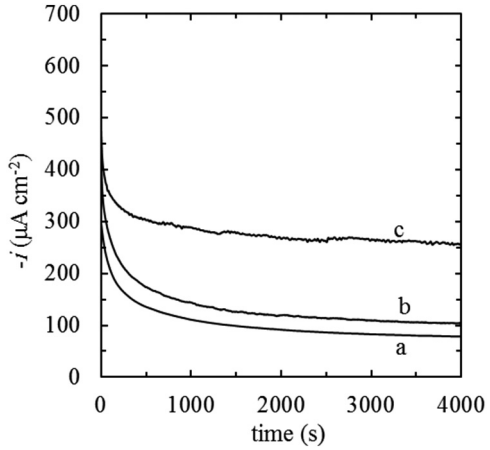

Fig. 8. Chronoamperometric curves of carbon steel at CP = −1.0 V_{SCE} at different temperatures: (a) 25 °C, (b) 35 °C, (c) 45 °C.

respectively, while the values of i_r are equal to 77, 104 and 254 μA cm^{-2}, respectively. Therefore, the temperature elevation is associated with the increase of scaling time, t_s and residual current density, i_r under the application of CP.

On the other hand, from the aspect of tendency for chemical deposition (in the absence of CP), the temperature favors the scaling kinetics leading to lower scaling times and also less residual current density due to higher coverage of metal surface by scale deposition. In fact, when the temperature of the solution increases, the solubility parameter, S, decreases according to Eqs. (4)–(7) and the carbonate concentration, $[CO_3^{2-}]$, increases (Eq. (8)) because of an increase in the pH_s value. In this situation (chemical deposition), an increase in tendency towards $CaCO_3$ deposition is expected.

This discrepancy can be explained by the different conditions encountered in chemical and electrochemical precipitation. In other words, the chemical deposition is controlled by two factors of solubility,

Table 5
Effect of $[HCO_3^-]$ on the impedance parameters for carbon steel cathodically polarized at −1.0 V_{SCE} in artificial seawater based on ASTM D1141.

$[HCO_3^-]_{Std}$ (%)	R_f (Ω cm^2)	CPE_f		R_{ct} (Ω cm^2)	CPE_{dl}	
		$Y_f \times 10^4$ (Ω^{-1} cm^{-2} s^n)	n_f		$Y_{dl} \times 10^4$ (Ω^{-1} cm^{-2} s^n)	n_{dl}
50	390	3.50	0.75	760	109	0.56
100	360	4.16	0.74	720	129	0.52
200	340	4.52	0.73	690	132	0.50

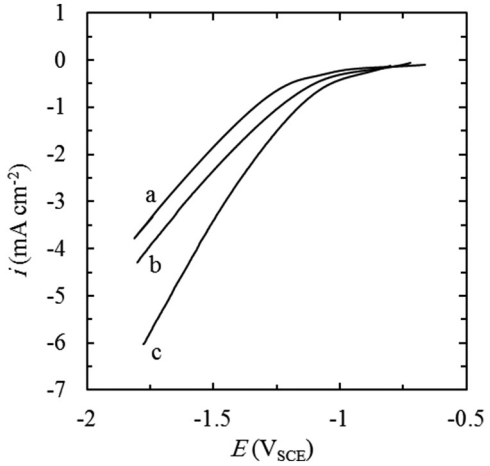

Fig. 9. Current-potential curves of carbon steel at CP = −1.0 V_{SCE} at different temperatures (a) 25 °C, (b) 35 °C, (c) 45 °C. Scan rate: 1 mV s^{-1}.

S and ion concentrations (here Ca^{2+} and CO_3^{2-}) within the bulk solution determined by thermodynamics equilibrium relations while, in the case of electrochemical deposition, the application of CP causes the interference of the hydrogen evolution phenomenon on $CaCO_3$ deposition and thus deviation from that is commonly predicted by the chemical precipitation.

To investigate the electrochemical deposition under temperature variation, the current-voltage curves registered at different solution temperatures are shown in Fig. 9. In the plateau region corresponding to oxygen reduction, the value of the current density decreases slightly with temperature which is in good agreement with findings in other similar works [21,22,32]. In fact, the temperature elevation is associated with an decrease in oxygen solubility and an increase in the diffusion coefficient [21]. However, it was reported that the effect of the latter is more important and thus accelerates the reduction rate of oxygen [22]. This can be considered as the reason for the slight shift of the curves towards the cathodic direction. Although, it should also be mentioned that the increase of O_2 reduction reaction does not have a significant impact on the interfacial pH [32].

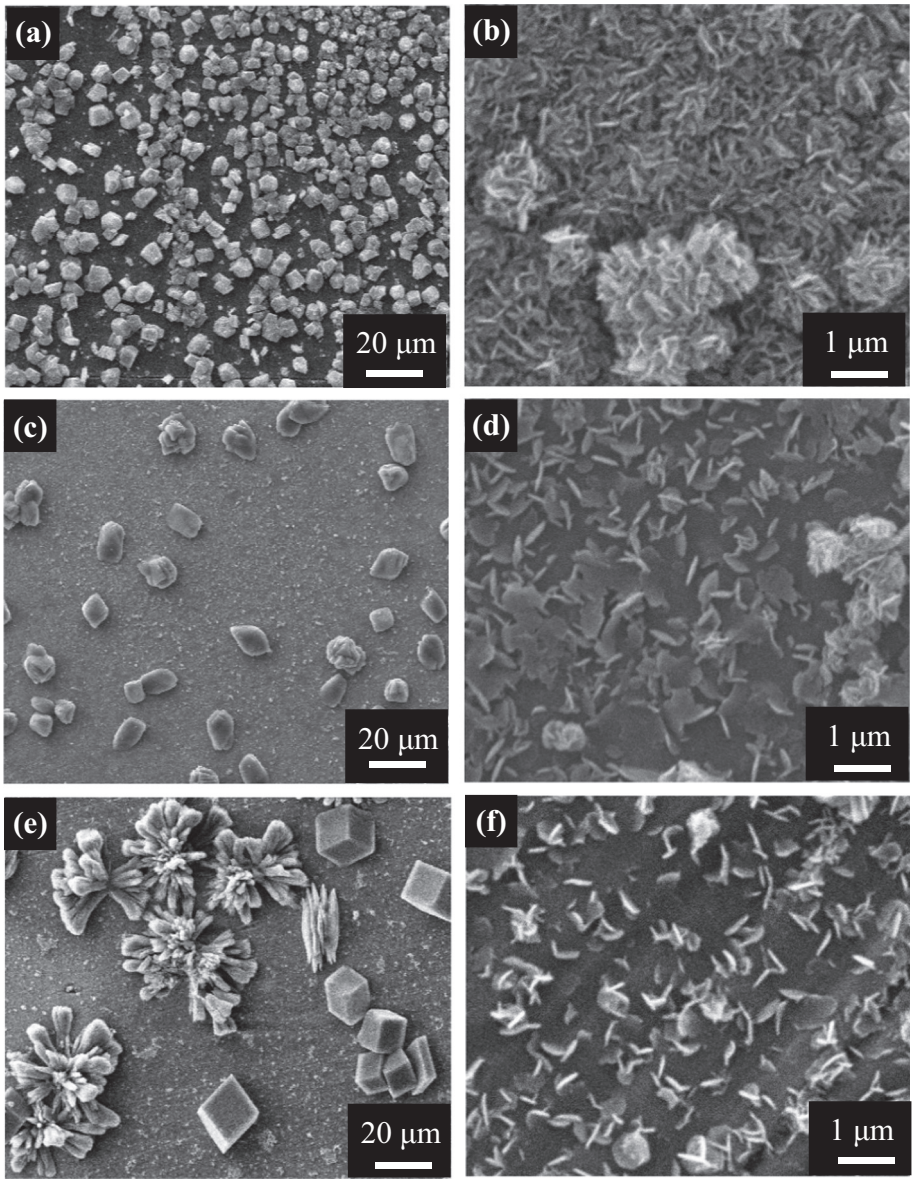

Fig. 10. SEM micrographs of carbon steel surface in artificial sea water based on ASTM D1141 at 25 °C after cathodically polarization at (a and b) −0.8 V_{SCE}, (c and d) −1.0 V_{SCE}, (e and f) −1.2 V_{SCE} at different magnifications.

A careful look at Fig. 9 reveals that the length of the diffusion plateau decreases with temperature suggesting that water reduction starts from more noble potentials and thus its contribution to the total reduction current density increases at CP = $-1.0\ V_{SCE}$. In addition, as discussed before, water reduction causes two effects on $CaCO_3$ precipitation: the first effect is the increase in the interfacial pH by producing a higher content of hydroxyl groups and the second is the increase in the rate of hydrogen bubbling. Considering these concepts, the increase of i_r and t_s with temperature obviously advises the predominant effect of the hydrogen evolution phenomenon on the scale precipitation under the application of CP. This interesting observation can be explained by the fact that the elevation of solution temperature (a) increases the contribution of water reduction from i_r, especially around the CP = $-1.0\ V_{SCE}$ and (b) stimulates water reduction reaction. These two effects ensure a higher rate of hydrogen evolution causing not only a reduction in the surface coverage but also an inhibiting effect of temperature elevation on the electrochemical $CaCO_3$ deposition.

An inspection of Fig. 8 reveals that when the solution temperature rises from 25 °C to 45 °C, the fluctuations in the cathodic current density increase which is evidence of the instability of the $CaCO_3$ film associated with the high rate of hydrogen bubbling. Therefore, the EIS test on the scale film may be unreliable in this condition.

3.5. Surface analyses

The effect of CP (-0.8, -1.0 and $-1.2\ V_{SCE}$) on the morphology of scale deposition on the carbon steel surface in the artificial seawater at 25 °C can be seen in Fig. 10 at two magnifications (2500 and 25,000). It appears that the $CaCO_3$ crystals are made of both small and large sizes regardless of the applied potentials. At the lower magnification, i.e. 2500 (Fig. 10a, c and e), the $CaCO_3$ crystals are made of two well-defined forms including calcite in a rhombohedral shape and aragonite in a cauliflower morphology [2]. It is apparent that the proportion of aragonite crystals to that of calcite is increased by the shift of CP towards the negative direction. The SEM images taken at higher magnification, i.e. 25,000 (Fig. 10b, d and f), show that a thin film of needle like aragonite crystals covers throughout the metal surface which is in good agreement with that was reported before [9]. Considering these observations, it can be stated that in both low and high magnifications, the compaction and thus the coverage percentage of the scale film decrease as a result of the application of more negative CP. This can be explained by the hindering effect of hydrogen evolution on both the nucleation and growth stages of the deposition process, thus confirming the results obtained in electrochemical tests.

The constituent elements of the scale layer deposited on the carbon steel surface were analyzed using the EDS technique whereas very similar spectra were obtained at different conditions. Thus, the EDS spectrum of the scale deposited on the carbon steel surface in artificial seawater at 25 °C after cathodically polarization at CP = $-1.0\ V_{SCE}$ (corresponding to Fig. 10c and d) is typically shown in Fig. 11. The presence of a significant peak for the calcium element confirms the formation of the $CaCO_3$ crystal which is in keeping with the results obtained in other similar studies [15].

To clarify the effect of temperature on the $CaCO_3$ precipitation, SEM photographs of the scale precipitated on the carbon steel surface at CP = $-1.0\ V_{SCE}$ and 45 °C are shown in Fig. 12 at two different magnifications. It is obvious that the deposit film is composed of a large calcite and small needle like aragonite crystals with approximately a sharp size distribution. When temperature increases from 25 °C to 45 °C, a comparison of SEM images taken at low and high magnifications shows that while the amount of calcite crystals increases, that of aragonite crystals decreases significantly. Indeed, the effect of temperature elevation on hydrogen bubbling can be explained as facilitation of nucleation and growing stages of calcite crystal and a reverse effect on those of the aragonite.

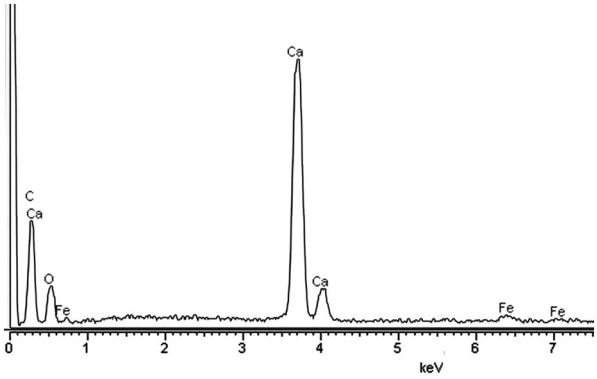

Fig. 11. Energy dispersive spectrum for deposit formed on carbon steel surface in artificial solution based on ASTM D1141 at 25 °C after cathodically polarization at $-1.0\ V_{SCE}$.

Regarding the chronoamperometric tests, it has been found that the residual current density (i_r) decreases with temperature due to the decreasing the coverage of metal surface as a result of hydrogen bubbling. Therefore, it can be concluded that the coverage property of the $CaCO_3$ scale depends mainly on aragonite crystals. This could be attributed to the fact of the smaller size of aragonite than that of calcite favoring formation a more compact film and probably higher adherent of aragonite crystals to the carbon steel surface.

4. Conclusion

In this study, the significant effect of the hydrogen evolution phenomenon on $CaCO_3$ deposition was investigated in artificial seawater under different conditions. The main findings of the present study are as follows:

- When the CP shifted towards negative values, the water reduction reaction had the main contribution to the i_r. The water reduction reaction is associated with the increase in both interfacial pH and hydrogen evolution while the latter had a major effect on the electrochemical deposition and significantly prevented the $CaCO_3$ precipitation.
- Interestingly enough, the increase of bicarbonate concentration caused the reduction in the coverage of metal surface by the scale deposition. This behavior can be explained as a competition between the increment of carbonate ions stimulating scale deposition and hydrogen evolution hindering the scale formation. However, the obtained results showed that the effect of hydrogen bubbling is predominant under electrochemical precipitation.
- The temperature rise also showed an inhibiting influence on $CaCO_3$ deposition under the application of CP. This interesting observation was at odds with the normal effect of temperature elevation on the scale deposition and can be explained as the predominant effect of hydrogen evolution. In fact, the temperature elevation causes the increase in the rate of hydrogen evolution under electrochemical precipitation by means of: (a) the increase in the contribution of water reduction to the i_r and (b) increase in the rate of water reaction.
- The SEM images showed that the scale deposition is made of both large sizes of calcite and small sizes of aragonite crystals. The quality of surface coverage of carbon steel confirmed the effect of hydrogen evolution obtained by electrochemical tests. However, it could be concluded that the coverage property of the scale film depends on the aragonite crystals to a large extent.

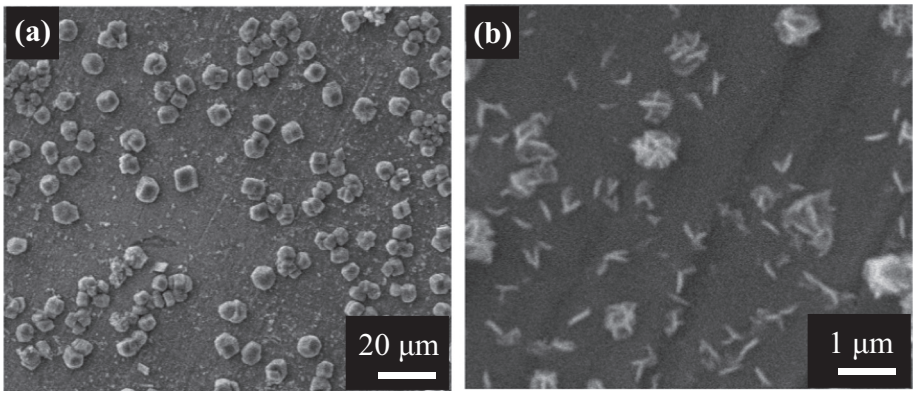

Fig. 12. SEM micrographs of carbon steel surface at 45 °C and CP = −1.0 V_{SCE} and at different magnifications.

References

[1] Y.P. Lin, P.C. Singer, Inhibition of calcite crystal growth by polyphosphates, Water Res. 39 (2005) 4835–4843.

[2] C. Barchiche, C. Deslouis, D. Festy, O. Gil, P. Refait, S. Touzain, B. Tribollet, Characterization of calcareous deposits in artificial seawater by impedance techniques, 3—Deposit of $CaCO_3$ in the presence of Mg (II), Electrochim. Acta 48 (2003) 1645–1654.

[3] A. Kavitha, T. Vasudevan, H.G. Prabu, Evaluation of synthesized antiscalants for cooling water system application, Desalination 268 (2011) 38–45.

[4] A. Abdel-Gaber, B. Abd-El-Nabey, E. Khamis, D. Abd-El-Khalek, Investigation of fig leaf extract as a novel environmentally friendly antiscalant for $CaCO_3$ calcareous deposits, Desalination 230 (2008) 314–328.

[5] S. Hoseinieh, T. Shahrabi, Influence of ionic species on scaling and corrosion performance of AISI 316 L rotating disk electrodes in artificial seawater, Desalination 409 (2017) 32–46.

[6] C. Gabrielli, G. Maurin, G. Poindessous, R. Rosset, Nucleation and growth of calcium carbonate by an electrochemical scaling process, J. Cryst. Growth 200 (1999) 236–250.

[7] S. Xin, M. Li, Electrochemical corrosion characteristics of type 316 L stainless steel in hot concentrated seawater, Corr. Sci. 81 (2014) 96–101.

[8] C. Garcia, G. Courbin, F. Ropital, C. Fiaud, Study of the scale inhibition by HEDP in a channel flow cell using a quartz crystal microbalance, Electrochim. Acta 46 (2001) 973–985.

[9] S. Ghizellaoui, M. Euvrard, Assessing the effect of zinc on the crystallization of calcium carbonate, Desalination 220 (2008) 394–402.

[10] D. Abd-El-Khalek, B. Abd-El-Nabey, Evaluation of sodium hexametaphosphate as scale and corrosion inhibitor in cooling water using electrochemical techniques, Desalination 311 (2013) 227–233.

[11] C. Barchiche, C. Deslouis, O. Gil, P. Refait, B. Tribollet, Characterisation of calcareous deposits by electrochemical methods: role of sulphates, calcium concentration and temperature, Electrochim. Acta 49 (2004) 2833–2839.

[12] S. Benslimane, H. Perrot, R. Bennezar, K.-E. Bouhidel, Thermodynamic study of Zn^{2+} inhibition properties and mechanism on calcium carbonate precipitation by chemical and electrochemical methods, Desalination 398 (2016) 114–120.

[13] J. Marin-Cruz, R. Cabrera-Sierra, M. Pech-Canul, I. Gonzalez, EIS study on corrosion and scale processes and their inhibition in cooling system media, Electrochim. Acta 51 (2006) 1847–1854.

[14] M. Tlili, M. Benamor, C. Gabrielli, H. Perrot, B. Tribollet, Influence of the interfacial pH on electrochemical $CaCO_3$ precipitation, J. Electrochem. Soc. 150 (2003) C765–C771.

[15] R. Ketrane, B. Saidani, O. Gil, L. Leleyter, F. Baraud, Efficiency of five scale inhibitors on calcium carbonate precipitation from hard water: effect of temperature and concentration, Desalination 249 (2009) 1397–1404.

[16] C. Barchiche, C. Deslouis, O. Gil, S. Joiret, P. Refait, B. Tribollet, Role of sulphate ions on the formation of calcareous deposits on steel in artificial seawater; the formation of Green Rust compounds during cathodic protection, Electrochim. Acta 54 (2009) 3580–3588.

[17] S. Lin, S. Dexter, Effects of temperature and magnesium ions on calcareous deposition, Corrosion 44 (1988) 615–622.

[18] C. Deslouis, D. Festy, O. Gil, G. Rius, S. Touzain, B. Tribollet, Characterization of calcareous deposits in artificial sea water by impedance techniques—I. Deposit of $CaCO_3$ without Mg $(OH)_2$, Electrochim. Acta 43 (1998) 1891–1901.

[19] T. Okstad, Ø. Rannestad, R. Johnsen, K. Nisancioglu, Significance of hydrogen evolution during cathodic protection of carbon steel in seawater, Corrosion 63 (2007) 857–865.

[20] C. Gabrielli, M. Keddam, A. Khalil, R. Rosset, M. Zidoune, Study of calcium carbonate scales by electrochemical impedance spectroscopy, Electrochim. Acta 42 (1997) 1207–1218.

[21] R. Lee, J. Ambrose, Influence of cathodic protection parameters on calcareous deposit formation, Corrosion 44 (1988) 887–891.

[22] H. Karoui, B. Riffault, M. Jeannin, A. Kahoul, O. Gil, M.B. Amor, M.M. Tlili, Electrochemical scaling of stainless steel in artificial seawater: role of experimental conditions on $CaCO_3$ and Mg $(OH)_2$ formation, Desalination 311 (2013) 234–240.

[23] K. Mantel, W. Hartt, T.-Y. Chen, Substrate, surface finish, and flow rate influences on calcareous deposit structure, Corrosion 48 (1992) 489–500.

[24] B.M. Tissue, Basics of Analytical Chemistry and Chemical Equilibria, John Wiley & Sons, 2013.

[25] D.A. Skoog, D.M. West, F.J. Holler, S.R. Crouch, Fundamentals of Analytical Chemistry, Cengage Learning (2014) 373.

[26] H.S. Harned, R. Davis Jr, The ionization constant of carbonic acid in water and the solubility of carbon dioxide in water and aqueous salt solutions from 0 to 50, J. Amer. Chem. Soc. 65 (1943) 2030–2037.

[27] H.S. Harned, S.R. Scholes Jr, The ionization constant of HCO_3- from 0 to 50, J. Amer. Chem. Soc. 63 (1941) 1706–1709.

[28] C. Gabrielli, R. Jaouhari, G. Maurin, M. Keddam, Magnetic water treatment for scale prevention, Water Res. 35 (2001) 3249–3259.

[29] C. Deslouis, I. Frateur, G. Maurin, B. Tribollet, Interfacial pH measurement during the reduction of dissolved oxygen in a submerged impinging jet cell, J. Appl. Electrochem. 27 (1997) 482–492.

[30] L. Paolinelli, T. Pérez, S. Simison, The effect of pre-corrosion and steel microstructure on inhibitor performance in CO_2 corrosion, Corr. Sci. 50 (2008) 2456–2464.

[31] F.F. Eliyan, E.-S. Mahdi, A. Alfantazi, Electrochemical evaluation of the corrosion behaviour of API-X100 pipeline steel in aerated bicarbonate solutions, Corr. Sci. 58 (2012) 181–191.

[32] C. Deslouis, D. Festy, O. Gil, V. Maillot, S. Touzain, B. Tribollet, Characterization of calcareous deposits in artificial sea water by impedances techniques: 2-deposit of Mg (OH)2 without $CaCO_3$, Electrochim. Acta 45 (2000) 1837–1845.